analytical chemistry

Article

pubs.acs.org/ac

Intracavity DNA Melting Analysis with Optofluidic Lasers

Wonsuk Lee[†,‡] and Xudong Fan*[,†]

[†]Department of Biomedical Engineering, University of Michigan, 1101 Beal Avenue, Ann Arbor, Michigan 48109, United States

[‡]Department of Electrical Engineering and Computer Science, University of Michigan, 1301 Beal Avenue, Ann Arbor, Michigan 48109, United States

Supporting Information

ABSTRACT: DNA melting analysis holds great promise for simple and fast DNA sequence discrimination. However, conventional fluorescence-based methods suffer from a small differential signal and demanding melting curve analysis, both of which make it difficult to distinguish the target DNA from the mismatched one. Herein, we propose and demonstrate a highly specific intracavity DNA melting analysis scheme utilizing an optofluidic laser. The laser optically amplifies the small yet intrinsic thermal dynamic difference between the target and the single-base-mismatched DNA, resulting in a differential signal that is orders of magnitude greater than with fluorescence-based methods. In particular, the existence of a phase transition between the stimulated laser emission and fluorescence (i.e., spontaneous emission) enables accurate determination of the DNA transition temperature difference. Furthermore, the high differential signal in the intracavity detection allows for scanning of the laser excitation at a fixed temperature to distinguish two DNA sequences, which provides another means for rapid DNA analysis. In this paper, we first theoretically investigate DNA melting analysis using an optofluidic laser and then experimentally explore this scheme with a high-quality optofluidic ring resonator. Distinction of two DNA sequences of up to 100 bases long is demonstrated. The intracavity detection developed here will lead to novel optofluidic devices that enable rapid and simple analysis of DNAs with very long sequences.

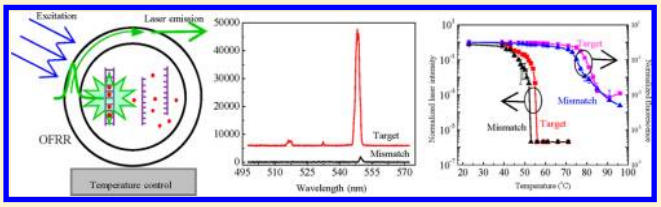

A DNA sequence may have a single-base change resulting from biological processes such as single-point mutation or cytosine methylation.[1,2] Distinguishing the sequential difference at the level of single-base-mismatch in DNAs can provide valuable information for disease diagnosis, medicine development, and genomic research.[3−9] High-resolution melting (HRM) analysis is a newly developed technology for analyzing DNA, in particular, after polymerase chain reaction (post-PCR), in a contamination-free closed-tube manner.[10−18] HRM relies on the thermal dynamic difference between the target and the single-base-mismatched DNA to distinguish them. As illustrated in Figure 1a, HRM employs fluorescence from intercalating saturation dyes as the sensing signal. The saturation dye, when bound to double-stranded DNA (dsDNA), has strong fluorescence. With increased temperature, dsDNAs dissociate into single-stranded DNAs (ssDNAs). As a result, the dye is released from the dsDNA strands and its fluorescence decreases. The DNA melting curve is acquired by monitoring the fluorescence as a function of temperature. The melting curve depends on the affinity between the two binding DNA strands, which is in turn determined by the length and the sequence of the DNA, as well as the number of base mismatches.

As compared to other DNA analysis methods, such as molecular beacons[19,20] and DNA arrays,[21] HRM is simple, fast, cost-effective, and easy to use. It does not require complicated and costly fluorophore labeling, and can be directly operated in free solution without involving surface immobilization of DNA probes. Particularly, in contrast to the molecular beacons and DNA arrays that can handle only short DNA sequences (~20−30 bases), HRM is capable of analyzing DNA sequences of hundreds of bases.[11,12,14] To date, HRM has been employed in single-nucleotide polymorphisms, mutation discovery, and viral/bacterial population diversity investigation. However, due to the small thermal dynamic difference between the target and mismatched DNA, the difference in fluorescence signal is usually very small (a few percent) and diminishes with the increased sequence length. Finding an optimized method to resolve the small yet intrinsic thermal dynamic difference is crucial in expanding the HRM capability for DNA analysis.

In this work, we attempt to amplify the thermal dynamic difference using an optical feedback provided by a laser cavity. Our scheme involves placing DNA samples and saturation dyes inside a microsized optofluidic laser cavity for intracavity detection. Instead of fluorescence, stimulated emission from the optofluidic laser is used as the sensing signal. When temperature varies, the laser gain (hence the laser output), which is determined by the DNA hybridization state, is modulated significantly. Our scheme offers a number of unique advantages: (1) Through an intracavity detection, the small yet intrinsic thermal dynamic difference between the target and the single-base-mismatched DNA can be optically amplified,

Received: August 21, 2012
Accepted: September 27, 2012
Published: September 27, 2012

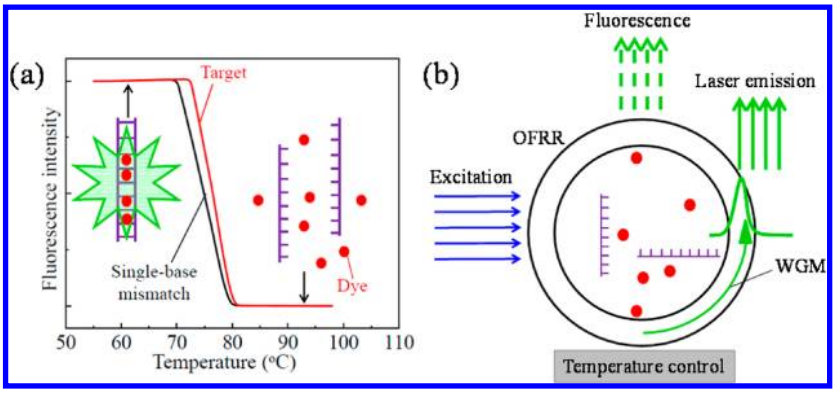

Figure 1. (a) DNA melting analysis with the intercalating saturation dye. The dye has strong fluorescence in the presence of dsDNA. As temperature increases, dsDNAs melt into ssDNAs. Consequently, fluorescence from the saturation dye diminishes. The target and the base-mismatched DNA can be discriminated by analyzing corresponding melting curves. (b) Schematic of the microcapillary OFRR laser. The WGM interacts evanescently with the dye flowing through the capillary and provides the optical feedback for lasing. The laser emission can be collected at the edge of the OFRR, whereas the conventional fluorescence can be collected concomitantly from the central part of the OFRR, which has no interaction with the WGM. A temperature control containing an electric heater and a thermal probe is placed outside the OFRR to change temperature. Dimensions are not to scale.

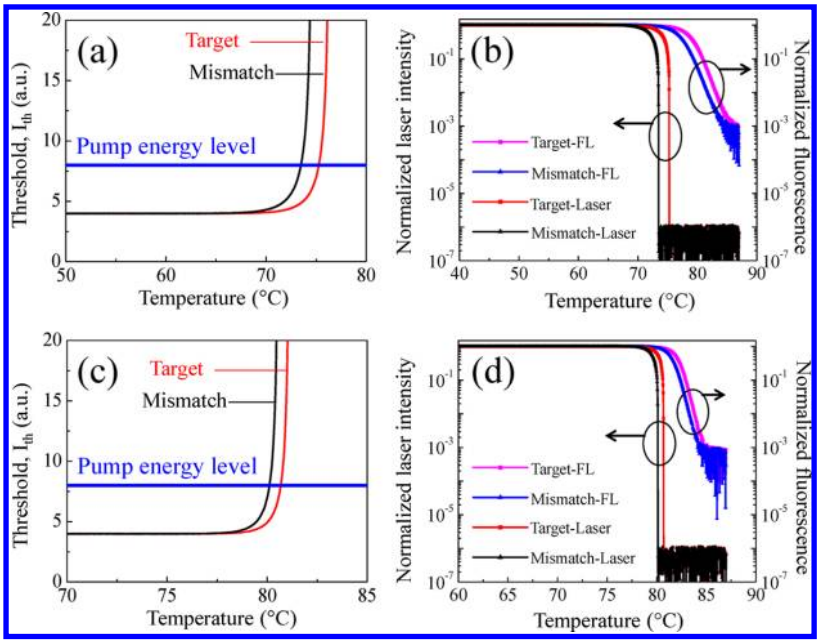

Figure 2. (a) Lasing threshold calculated for the target and the single-base-mismatched DNA with 40 bases using eq 1. (b) The corresponding normalized laser output intensity and fluorescence using eqs 4 and 5. (c) Lasing threshold calculated for the target and single-base-mismatched DNA with 100 bases using eq 1. (d) The corresponding normalized laser output intensity and fluorescence using eqs 4 and 5. All the DNA sequences are listed in Table S1 in the Supporting Information. All curves are normalized to their respective maximal intensity at 23 °C. The laser transition temperature, at which the laser intensity drops to zero, is (b) 75.25 °C (73.52 °C) and (d) 80.68 °C (80.11 °C) for the target (single-base-mismatch). In panels a and c, γ is set to be 0.8. In panels b and d, the same level of instrument noise is added to both laser output and fluorescence. Note that the relative noise level in the laser output appears to be orders of magnitude lower than that in fluorescence due to the fact that the laser output intensity is much higher than fluorescence.

resulting in orders of magnitude improvement in the differential signal (the emission ratio between the target and the mismatched DNA). (2) When temperature varies, the laser undergoes a sharp phase transition from stimulated laser emission to regular fluorescence (i.e., spontaneous emission), which allows us to precisely determine the DNA transition temperature difference between the target and the mismatched DNA. (3) In addition to temperature ramping as in the conventional melting analysis, the high differential signal allows us to scan the laser excitation at fixed temperature to distinguish two DNA sequences, which provides another means for rapid DNA analysis. In this paper, we first theoretically investigate DNA melting analysis using an optofluidic laser and then experimentally demonstrate this scheme with an optofluidic ring resonator (OFRR).

THEORETICAL ANALYSIS

According to the laser theory,[22,23] the lasing threshold, I_{th}, is determined by

$$I_{th} = \frac{\gamma}{\Gamma - \gamma} \quad (1)$$

dx.doi.org/10.1021/ac302416g | Anal. Chem. 2012, 84, 9558−9563

where γ is the required fraction of the dye molecules in the excited state at the onset of lasing, which is determined by the properties of the dye (such as dye absorption/emission cross section and total concentration), and the laser cavity (such as Q-factor).[23−26] Γ is the fraction of the dye molecules that participate in the lasing action, i.e.,

$$\Gamma = \frac{n_{\mathrm{dsDNA}}}{n_{\mathrm{T}}} \tag{2}$$

where n_{T} is the total concentration of the dye. n_{dsDNA} is the concentration of the dye that binds to the dsDNA and should be proportional to the dsDNA concentration, [dsDNA], which is in turn given by

$$[\mathrm{dsDNA}] \overset{K_{\mathrm{d}}}{\Leftrightarrow} [\mathrm{ssDNA}] \tag{3}$$

where K_{d} is the temperature-dependent dissociation constant and can be calculated using the standard method based on nearest-neighbor thermal dynamics for any given DNA sequence and temperature.[27,28] Detailed calculation of Γ is described in section I in the Supporting Information. For the laser output intensity, it is linearly proportional to the external pump energy level, I_{pump}, above the lasing threshold,[22] i.e.,

$$I_{\mathrm{output}} \propto \left(\frac{I_{\mathrm{pump}}}{I_{\mathrm{th}}} - 1\right) = I_{\mathrm{pump}}\left(\frac{\Gamma}{\gamma} - 1\right) - 1 \tag{4}$$

Through eqs 1−4, we can gain insight into how the optofluidic laser can be controlled by DNA thermal dynamics. Note that Γ also reflects the fluorescence intensity from the dye in the conventional DNA melting analysis, i.e.,

$$I_{\mathrm{output}} \propto \Gamma \tag{5}$$

Equations 4 and 5 allow us to compare the melting curves obtained with the intracavity detection and the conventional fluorescence method, respectively.

Figure 2a shows the calculated lasing thresholds as a function of temperature for the target DNA of 40 bases long and its single-base-mismatched counterpart (see Table S1 in the Supporting Information for the details of the DNA sequences). At a relatively low temperature, the external pump energy level (I_{pump}) is higher than the corresponding lasing threshold for the target and the mismatched DNA. Consequently, lasing emission should occur for both samples. As temperature increases, the lasing threshold increases rapidly due to decreased Γ. At the temperature where the threshold becomes higher than the given pump energy level, the laser output ceases, indicating a phase transition from laser emission to regular fluorescence with orders of magnitude change in output intensity. According to eqs 1−3, the target DNA always has a slightly higher transition temperature than the mismatched DNA for a given pump energy level, which is shown in Figure 2a. In addition, as long as I_{pump} is sufficiently high (i.e., well above the lasing threshold), the difference in the transition temperature is independent of I_{pump} (see Figure 2a). These characteristics, along with the sharp phase transition, allow us to accurately determine the transition temperature difference for clear distinction between the target and the mismatched DNA, as discussed next.

Figure 2b plots the normalized laser emission corresponding to Figure 2a. As compared to the fluorescence-based melting curve, the prevailing feature in the laser emission based melting curve is the sharp phase transition at which the emitted light intensity changes drastically. This cutoff behavior provides an extremely high differential signal (i.e., the emission ratio between the target and the mismatched DNA; see Figure S1 in the Supporting Information) and enables accurate determination of the difference in transition temperature in actual experiments. On the basis of Figure 2b, the transition temperature difference is approximately 1.73 °C obtained with the laser emission, close to the difference of 1.70 °C in the DNA melting temperature calculated with the fluorescence method (DNA melting temperature is defined as the temperature at which the fluorescence drop to 50% of its maximum at a low temperature). Another important feature is that laser emission based melting curves exhibit appreciable difference between the target and the mismatched DNA at a lower temperature at which the melting curves from the conventional method still remain virtually the same (e.g., 72 °C in Figure S1a in the Supporting Information), highlighting the underlying optical amplification mechanism of the intracavity detection.

To mimic the actual measurement, the same level of noise is added to both laser emission and fluorescence as the instrument noise (such as ambient light noise and detector's noise, etc.). Since the laser emission is orders of magnitude stronger than fluorescence, the relative impact of the noise on the laser emission based melting curve (particularly, around the sharp phase transition region) becomes negligible. In contrast, the fluorescence-based melting curve is much more susceptible to noise, which drastically affects the determination of melting temperature difference and the overall curve shape, especially when (1) longer DNA sequences are to be distinguished (in which case the fluorescence difference becomes smaller) and (2) low sample volumes are used (in which case the fluorescence becomes weaker).

Parts c and d of Figure 2 show the lasing thresholds and the laser/fluorescence intensities corresponding to the target and the single-base-mismatched DNA of 100 bases long, respectively. As compared to the 40 bases long DNA, the phase transition occurs at a higher temperature, as expected. While the transition temperature differences become smaller, the differential signal (see Figure S1 in the Supporting Information) remains equally large and is not degraded by the noise. It should be emphasized that the theoretical analysis and the intracavity detection principle discussed here are generally applicable to any optofluidic laser cavities, such as a ring resonator,[29−31] Fabry−Perot cavity,[32,33] and distributed feedback laser cavity.[34,35]

MATERIALS AND METHODS

In this paper, we use the OFRR to demonstrate intracavity DNA melting analysis. As illustrated in Figure 1b, the OFRR is based on a thin-walled fused-silica microcapillary, whose cross section forms a ring resonator that supports the whispering gallery mode (WGM) circulating along the capillary circumference.[23,29,36] The WGM interacts evanescently with the sample solution of the DNA and the saturation dye flowing through the OFRR, which provides an optical feedback for the dye to lase. Details of the OFRR fabrication, experimental setup, and sample preparation are described as follows.

Fabrication of the OFRR. The microcapillary OFRR is fabricated with a pre-etched fused-silica capillary preform (Polymicro Technologies, TSP700850) by the conventional drawing method reported previously.[23,29,36] Briefly, the fused-silica capillary with an outer diameter and inner diameter of 850

dx.doi.org/10.1021/ac302416g | Anal. Chem. 2012, 84, 9558−9563

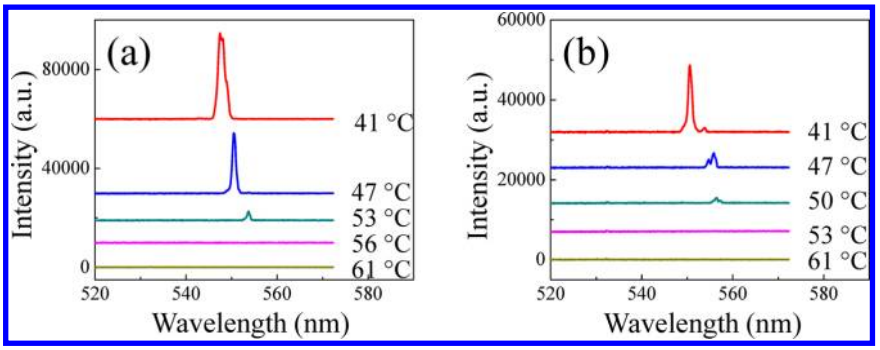

Figure 3. Examples of the lasing spectra for (a) the target DNA of 40 bases long and (b) the corresponding single-base-mismatched DNA above and below their respective laser transition temperature. The pump energy density is 980 μJ/mm^2 per pulse. Curves are vertically shifted for clarity. The DNA sequences are listed in Table S1 in the Supporting Information.

and 700 μm, respectively, is wet-etched with 5% hydrofluoric acid for 48 h and pulled under CO_2 laser radiation. The outer diameter and the wall thickness of the microcapillary after the pulling process are 80 and 5 μm, respectively.

Sample Preparation. The linearly structured DNA sequences used in the experiments (the target DNA and the single-base-mismatched DNA of 21, 40, and 100 bases long) are given in Table S1 in the Supporting Information. SYTO 13 nucleic acid stain (Invitrogen, originally dissolved in DMSO with 5 mM concentration) is used as the saturation dye and is separately mixed to the target and the mismatch samples. The mixture of DNA and the saturation dye is dissolved in the buffer solution (Tris−acetate−EDTA buffer, pH = 8.3) with the final concentration of 250 μM for DNA samples and the saturation dye.

Experimental Setup. The OFRR is pumped with an optical parametric oscillator (Continuum, 5 ns pulsed laser, wavelength = 488 nm, repetition rate = 20 Hz) while the fused-silica capillary is being filled with the sample solution. The external light source is focused onto the OFRR part of the microcapillary with a spot size of 3.8 mm^2, and the pump energy density is controlled by a neutral density filter. The laser signal and the fluorescence emission free-space-coupled into the multimode fiber are measured by the spectrometer (HR550i, Horiba Jobin Yvon), simultaneously.

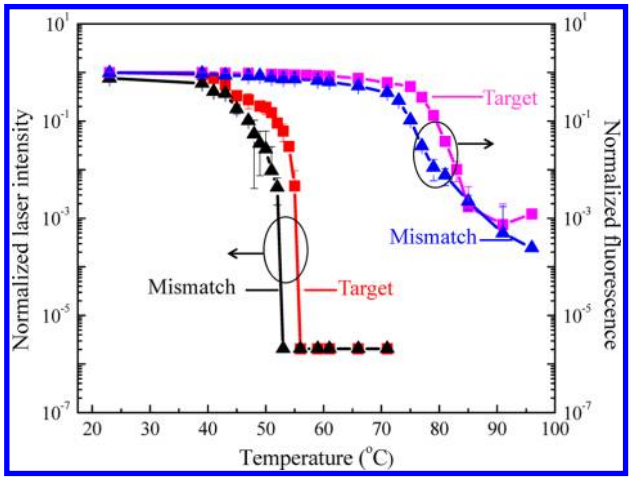

Figure 4. Spectrally integrated lasing intensity for the target and the single-base-mismatched DNA extracted from Figure 3 as a function of temperature with a finer temperature increment. The lasing transition, at which point the laser signal disappears, occurs at approximately 56 and 53 °C for the target and the single-base-mismatched DNA, respectively. For comparison, conventional fluorescence signals that are acquired concomitantly with the laser signals are also plotted. All curves are normalized to the respective target intensity at 23 °C. Error bars are obtained by five measurements.

RESULTS AND DISCUSSION

Figure 3 presents the laser emission spectra from the 40 bases long target and the corresponding single-base-mismatched DNA at various temperatures. At low temperature, both samples show the signature multimode lasing emission peaks (see Figure S2 in the Supporting Information for a higher resolution laser spectrum). With increased temperature, the laser intensity for both the target and the mismatched DNA decreases and eventually disappears, indicative of a phase transition from laser emission to fluorescence. The distinct difference in the transition temperature between the target and the mismatched DNA is obvious. For example, the laser emission from the target DNA still persists at 53 °C (see Figure 3a), whereas the mismatched DNA shows no lasing signal at this temperature (see Figure 3b).

Figure 4 shows the OFRR laser-based DNA melting curves extracted from the spectra in Figure 3 with a finer temperature increment. Meanwhile, the fluorescence-based DNA melting curves are also obtained simultaneously under otherwise the same conditions (see Figure 1b). Overall, both the laser emission and the fluorescence curves agree qualitatively with the respective theoretical predictions in Figure 2.[37] For the fluorescence-based melting curves, the melting temperature of the target and the mismatched DNA is 72 and 68 °C, respectively, which is further verified by a commercial DNA melting analysis instrument (Chromo4 CFB-3240G, Biorad). In contrast, the laser emission exhibits a very sharp transition, with the transition temperature difference of approximately 3 °C. The maximal differential signal is over 10^4 around the phase transition temperature (~53 °C) for intracavity detection, whereas the differential signal is only 1.4 at the melting temperature (~68 °C) and is approximately 10 at best across the entire temperature range for the conventional detection. Furthermore, the relative noise level is dramatically reduced for the laser emission due to its orders-of-magnitude higher signal intensity. Figure S3 in the Supporting Information shows the differential signal extracted from Figure 4, which agrees qualitatively with the theoretical analysis in Supporting Information Figure S1.

Once the transition temperature is determined for a given target and its corresponding mismatch, the DNA can also be differentiated by scanning the excitation energy while keeping

dx.doi.org/10.1021/ac302416g | Anal. Chem. 2012, 84, 9558−9563

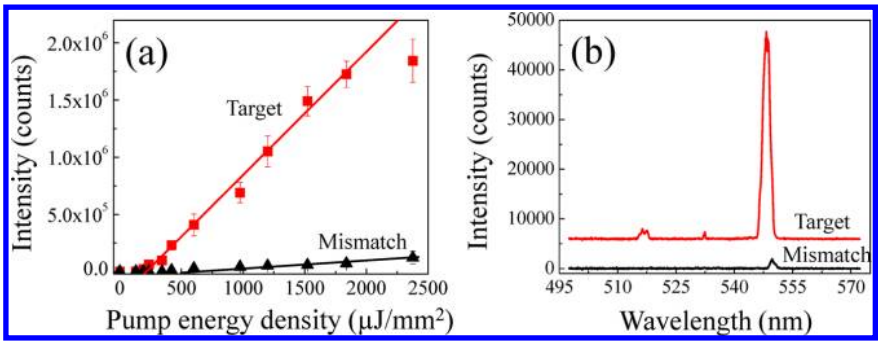

Figure 5. (a) Spectrally integrated lasing intensity as a function of pump energy density for the target and the single-base-mismatched DNA listed in Table S1 in the Supporting Information, when the temperature is fixed to 51 °C. The signal from the target DNA has a lasing threshold of approximately 216 μJ/mm^2 and shows typical lasing characteristics with a high lasing efficiency. The signal from the mismatch has a lasing threshold of approximately 500 μJ/mm^2 and shows only small lasing signal, even at high pump intensities. Solid lines are the linear fit above the threshold. (b) Representative lasing spectra at 51 °C for the target and the mismatch when the pump intensity is 1.84 mJ/mm^2. The integrated lasing intensity of the target DNA shows approximately 25 times higher than that of the single-base-mismatched DNA. The curves are vertically shifted for clarity. Error bars are obtained by five measurements.

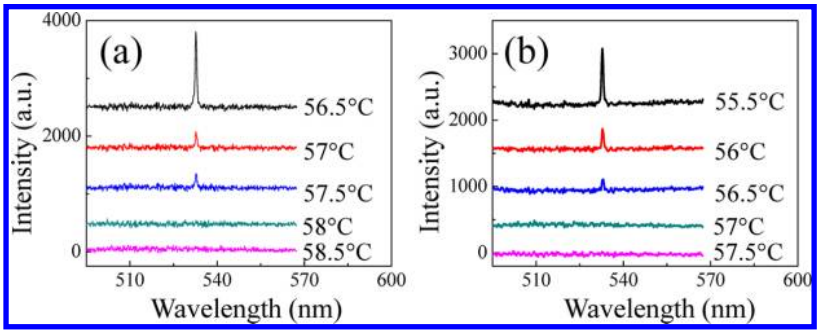

Figure 6. Lasing spectra for (a) the target DNA of 100 bases long and (b) the corresponding single-base-mismatched DNA above and below their respective laser transition temperature. The two samples show the transition temperature difference of approximately 1 °C. The pump energy density is 0.8 mJ/mm^2 per pulse. Curves are vertically shifted for clarity. The DNA sequences are listed in Table S1 in the Supporting Information.

the temperature constant. Figure 5a presents the spectrally integrated laser intensities for the same target and mismatched DNA used in Figures 3 and 4 when temperature is fixed at 51 °C. The target shows a clear laser characteristic with a lasing threshold of 216 μJ/mm^2 and high lasing efficiency of 1100 per μJ/mm^2, while the mismatch has a much higher lasing threshold of 500 μJ/mm^2 with lasing efficiency of only 70 per μJ/mm^2. Due to the large difference between the signals from the target and the mismatch, it may be even possible to distinguish the target from the mismatch without scanning the pump at all. This is exemplified by Figure 5b where the pump energy density is 1.84 mJ/mm^2. The integrated laser intensity for the target is approximately 25 times higher than that for the mismatch. Such large difference can only be obtained with the optical amplification. For comparison, the difference between the target and the mismatched DNA is only 10% at the same temperature for the conventional fluorescence detection, according to Figure 4. Note that the clearly distinguishable optical signal can be obtained with only one laser pulse excitation, which makes DNA detection much faster and simpler. In particular, for shorter DNA sequences, the DNA can even be distinguished at room temperature with the laser emission (see Supporting Information Figure S4), while conventional melting curve analysis shows virtually no difference (see Supporting Information Figure S5), isothermally.

We now move to validate the intracavity detection principle with even longer DNA sequences. Figure 6 illustrates the lasing spectra for the target DNA and the single-base-mismatched DNA with 100 bases long when the pump energy density is fixed at 0.8 mJ/mm^2. The melting curves show very similar temperature dependence in comparison with the previous results using 40 bases long DNAs (see Figure 3). The transition temperature of the target and the mismatch increases to approximately 57.5 and 56.5 °C, respectively. Although the transition temperature difference decreases to 1 °C, the target and the mismatched DNA can still be clearly distinguished by the cutoff behavior at their respective phase transition temperature.

CONCLUSION

We have analyzed and demonstrated the intracavity DNA detection method based on the OFRR laser. This novel scheme takes advantage of a sharp phase transition between laser emission and fluorescence, thus achieving an unprecedented differential signal between the target and the single-base-mismatched DNA, as well as accurate determination of the DNA transition temperature difference. Furthermore, the high differential signal enables rapid DNA analysis isothermally, where the laser excitation can be scanned. Finally, because of its high compatibility with well-developed microfluidic technologies,[31] the intracavity DNA melting analysis can be incorporated with on-chip PCR and other microfluidic components for lab-on-a-chip biosensing applications and micrototal analysis systems. Future work will include integration with on-chip

dx.doi.org/10.1021/ac302416g | Anal. Chem. 2012, 84, 9558−9563

droplet-based PCR and analysis of much longer DNA sequences (~1000 bases).

■ ASSOCIATED CONTENT

Supporting Information

Additional information as noted in text. This material is available free of charge via the Internet at http://pubs.acs.org.

■ AUTHOR INFORMATION

Corresponding Author

*E-mail: xsfan@umich.edu. Phone: 1-734-763-1273. Fax: 1-734-647-4834.

Notes

The authors declare no competing financial interest.

■ ACKNOWLEDGMENTS

We acknowledge support from the National Science Foundation (CBET-1037097 and ECCS-1045621) and the help of Dr. Yusuf Esmail Murgha and Professor Erdogen Gulari for using a real-time PCR instrument.

■ REFERENCES

(1) Wang, D. G.; Fan, J.-B.; Siao, C.-J.; Berno, A.; Young, P.; Sapolsky, R.; Ghandour, G.; Perkins, N.; Winchester, E.; Spencer, J.; Kruglyak, L.; Stein, L.; Hsie, L.; Topaloglou, T.; Hubbell, E.; Robinson, E.; Mittmann, M.; Morris, M. S.; Shen, N.; Kilburn, D.; Rioux, J.; Nusbaum, C.; Rozen, S.; Hudson, T. J.; Lipshutz, R.; Chee, M.; Lander, E. S. *Science* **1998**, *280*, 1077−1082.

(2) Jones, P. A.; Baylin, S. B. *Nat. Rev. Genet.* **2002**, *3*, 415−428.

(3) Christopoulos, T. K. *Anal. Chem.* **1999**, *71*, 425−438.

(4) Kelley, S. O.; Boon, E. M.; Barton, J. K.; Jackson, N. M.; Hill, M. G. *Nucleic Acids Res.* **1999**, *27*, 4830−4837.

(5) Shastry, B. S. *Pharmacogenomics* **2006**, *6*, 16−21.

(6) Zeglis, B. M.; Barton, J. K. *Nat. Protoc.* **2007**, *2*, 357−371.

(7) Veer, L. J. v. t.; Bernards, R. *Nature* **2008**, *452*, 564−570.

(8) Hawkins, A. R.; Schmidt, H. *Handbook of Optofluidics*; CRC Press: Boca Raton, FL, 2010.

(9) Chen, Z.; Qian, S.; Chen, X.; Chen, J.; Lina, Y.; Liud, J. *RSC Adv.* **2012**, *2*, 2562−2567.

(10) Erali, M.; Wittwer, C. T. *Methods* **2010**, *50*, 250−261.

(11) Montgomery, J.; Wittwer, C. T.; Palais, R.; Zhou, L. *Nat. Protoc.* **2007**, *2*, 59−66.

(12) Reed, G. H.; Wittwer, C. T. *Clin. Chem.* **2004**, *50*, 1748−1754.

(13) Sundberg, S. O.; Wittwer, C. T.; Greer, J.; Pryor, R. J.; Elenitoba-Johnson, O.; Gale, B. K. *Biomed. Microdevices* **2007**, *9*, 159−166.

(14) Wittwer, C. T.; Reed, G. H.; Gundry, C. N.; Vandersteen, J. G.; Pryor, R. J. *Clin. Chem.* **2003**, *49*, 853−860.

(15) Gudnason, H.; Dufva, M.; Bang, D. D.; Wolff, A. *Nucleic Acids Res.* **2007**, *35*, e127.

(16) López, C. M. R.; Asenjo, B. G.; Lloyd, A. J.; Wilkinson, M. J. *Anal. Chem.* **2011**, *82*, 9100−9108.

(17) Monis, P. T.; Giglio, S.; Saint, C. P. *Anal. Biochem.* **2005**, *340*, 24−34.

(18) Chen, N.; Tranebjærg, L.; Rendtorff, N. D.; Schrijver, I. *J. Mol. Diagn.* **2011**, *13*, 416−426.

(19) Tyagi, S.; Kramer, F. R. *Nat. Biotechnol.* **1996**, *14*, 303−308.

(20) Marras, S. A.; Kramer, F. R.; Tyagi, S. *Methods Mol. Biol. (N. Y.)* **2003**, *212*, 111−128.

(21) Sassolas, A.; Leca-Bouvier, B. D.; Blum, L. J. *Chem. Rev.* **2008**, *108*, 109−139.

(22) Siegman, A. E. *Lasers*; University Science Books: Sausalito, CA, 1986.

(23) Sun, Y.; Fan, X. *Angew. Chem., Int. Ed.* **2012**, *51*, 1236−1239.

(24) Lacey, S.; White, I. M.; Sun, Y.; Shopova, S. I.; Cupps, J. M.; Zhang, P.; Fan, X. *Opt. Express* **2007**, *15*, 15523−15530.

(25) Li, Z.; Psaltis, D. *Microfluid. Nanofluid.* **2008**, *4*, 145−158.

(26) Moon, H.-J.; Chough, Y.-T.; An, K. *Phys. Rev. Lett.* **2000**, *85*, 3161−3164.

(27) SantaLucia, J., Jr. *Proc. Natl. Acad. Sci. U.S.A.* **1998**, *95*, 1460−1465.

(28) Zuker, M. *Nucleic Acids Res.* **2003**, *31*, 3406−3415.

(29) Shopova, S. I.; Zhu, H.; Fan, X. *Appl. Phys. Lett.* **2007**, *90*, 221101.

(30) Suter, J. D.; Sun, Y.; Howard, D. J.; Viator, J. A.; Fan, X. *Opt. Express* **2008**, *16*, 10248−10253.

(31) Lee, W.; Luo, Y.; Zhu, Q.; Fan, X. *Opt. Express* **2011**, *19*, 19668−19674.

(32) Helbo, B.; Kristensen, A.; Menon, A. *J. Micromech. Microeng.* **2003**, *13*, 307−311.

(33) Vezenov, D. V.; Mayers, B. T.; Conroy, R. S.; Whitesides, G. M.; Snee, P. T.; Chan, Y.; Nocera, D. G.; Bawendi, M. G. *J. Am. Chem. Soc.* **2005**, *127*, 8952−8953.

(34) Li, Z. Y.; Zhang, Z. Y.; Emery, T.; Scherer, A.; Psaltis, D. *Opt. Express* **2006**, *14*, 696−701.

(35) Song, W.; Vasdekis, A. E.; Li, Z.; Psaltis, D. *Appl. Phys. Lett.* **2009**, *94*, 051117.

(36) Sun, Y.; Shopova, S. I.; Wu, C.-S.; Arnold, S.; Fan, X. *Proc. Natl. Acad. Sci. U.S.A.* **2010**, *107*, 16039−16042.

(37) Note that we are not intended to compare quantitatively the experimental results with the theoretical ones, as the melting curves depends highly on other parameters such as the salt concentration and the mismatch position in the sequence.